JOURNAL OF Materials CHEMISTRY

Cation doping and oxygen diffusion in zirconia: a combined atomistic simulation and molecular dynamics study

M. Sakib Khan,[a] M. Saiful Islam*[a] and David R. Bates[b]

[a] *Department of Chemistry, University of Surrey, Guildford, UK GU2 5XH*
[b] *BG Technology, Gas Research and Technology Centre, Ashby Road, Loughborough, UK LE11 3GR*

Received 26th May 1998, Accepted 8th July 1998

Computer simulation techniques have been used to investigate the defect and transport properties of the zirconia (ZrO_2) oxygen-ion conductor. First, a wide variety of low-valent metal ions are substituted into zirconia, and the energetics of solution investigated. Favourable dopants (on energetic grounds) have been calculated and include CaO, Y_2O_3, Gd_2O_3, and Sc_2O_3 in agreement with observation. Dopant-vacancy clusters are also examined with the results revealing trends with dopant ion size and significant local atomic relaxation. These simulations are extended to encompass the topical area of Nb/Y co-doping in zirconia. Oxygen ion diffusion in yttria-stabilised zirconia is studied by application of molecular dynamics (MD) techniques; our results support models in which diffusion is mediated by oxygen vacancies, with calculated diffusion coefficients and activation energies in accord with tracer diffusion studies.

Interest in materials that exhibit high oxygen ion mobility has increased considerably over the last two decades. One of the primary reasons for this interest is that many new and developing technologies, such as fuel cells and oxygen separators, depend on the greater understanding of the defect and ion transport processes in these materials.[1,2] It is well established that doping fluorite-structured zirconia (ZrO_2) with aliovalent cations (*e.g.* Y^{3+}, Ca^{2+}) increases the number of charge-compensating oxygen vacancies which are directly responsible for the ionic conduction in this system.[3–5] Indeed, stabilised ZrO_2 has found many uses as an electrolyte in solid oxide fuel cells (SOFC) and within oxygen sensors and generators, owing to its high oxygen ion conductivity.[1,5–8]

It is clear that dopant incorporation has a major influence on the transport behaviour of oxygen ion conductors such as ZrO_2. However, the precise defect structure of doped or stabilised ZrO_2 is still not fully characterised. Conductivity studies have shown that higher dopant concentrations (>10%) produce an increase in activation energy (and decrease in ionic conductivity), which is thought to arise from some form of vacancy-dopant association that traps the migrating oxygen vacancies.[9] There has been much debate on the nature of the interaction between the dopant cation and charge-compensating vacancies to form distinct defect clusters. It has been suggested that the oxygen vacancies sit at nearest-neighbour (NN) sites to the dopant ion, giving them seven-fold coordination.[10,11] In contrast, some studies indicate that anion vacancies sit on next-nearest-neighbour (NNN) sites with respect to the dopant, leading to eight-fold coordination of the dopant, but seven-fold coordination of Zr^{4+} which is similar to its environment in monoclinic zirconia.[12,13] It is therefore clear that consideration of the local atomic structure is crucial in order to fully understand the effect of dopants in this material.

In an attempt to determine the defect and transport properties of ZrO_2, a combination of defect simulation and molecular dynamics (MD) techniques have been applied, which are well suited to the study of electroceramics on the microscopic scale; these techniques are now established tools in the field of solid state chemistry and have been applied to other oxygen ion conductors such as the $LaMO_3$ (M = Co, Mn, Ga) perovskites.[14] In addition to the defect calculations, we have examined oxygen ion diffusion in doped zirconia using MD techniques which are particularly suited to probing ion transport properties. The temperature and concentration of charge carriers can have a direct effect on ion diffusion and can be modelled by MD methods; the results obtained are also directly comparable with experimental diffusion data. Whereas static lattice methods are used to probe the energetics and pathway of a single migrating ion, the MD approach can view the time evolution of the whole system.

In the present study, we have focused our attention on the energetics of dopant substitution, of dopant-vacancy clustering, and on the mechanistic features of oxygen ion transport; this extends previous simulation studies on the ZrO_2 system[15] by considering a wider range of dopants, together with the interesting issue of Nb/Y co-doping.

Simulation methods

The simulations are formulated within the framework of the Born model, the main features of which are the nature of the interatomic potentials and the modelling of perfect and defective lattices. The present account of these widely used techniques (embodied in the GULP code[16] for the lattice simulations and in the DLPOLY code[17] for the molecular dynamics calculations) will be brief since comprehensive reviews are given elsewhere.[18,19]

The effective potentials describing the interatomic forces are represented by ionic, pair-wise potentials of the form

$$\Phi_{\alpha\beta}(r) = \frac{-Z_\alpha Z_\beta e^2}{\varepsilon r} + A_{\alpha\beta}\exp(-r/\rho_{\alpha\beta}) - C_{\alpha\beta}/r^6 \qquad (1)$$

which includes a long-range Coulombic interaction, and a short-range term to model the repulsions and van der Waals attractions between electron charge clouds. Because charged defects will polarise other ions in the lattice, ionic polarisability must be incorporated into the potential model. The shell model provides a simple description of such effects and has also proven to be effective in simulating the dielectric properties of ceramic oxides.

An important feature of these calculations is the treatment of lattice relaxation about the point defect or migrating ion. The Mott–Littleton approach is to partition the crystal lattice into two regions so that ions in a spherical inner region (I) surrounding the defect are relaxed explicitly.[18] In contrast, the

remainder of the crystal, where the defect forces are relatively weak, is treated by more approximate quasi-continuum methods. In this way local relaxation is modelled effectively and the crystal is not considered simply as a rigid lattice through which ion species diffuse.

The potential parameters for the Zr–O and O–O interactions were transferred directly from the analogous simulation study of ZrO_2.[15] Table 1 lists the interatomic potentials and shell model parameters used in this study. The calculated bond distances and lattice parameters and their comparison with experimental values are listed in Table 2. Examination of the differences shows good agreement between experimental and simulated structures, as well as reasonable accord with the measured dielectric constant (relative permittivity).

The MD technique consists of an explicit dynamical simulation of the ensemble of particles for which Newton's equations of motion are solved. Repetition of the integration algorithm yields a detailed picture of the evolution of the system as a function of time. As with most MD studies to date, the shell model to treat ionic polarisation has not been employed. In the case of the cations this should lead to negligible errors, although the polarisability of the O^{2-} ion will be significant and is expected to be the major shortcoming of the potential model. It is worth noting that the shell model MD study of CaF_2 found that the explicit inclusion of polarisability had little effect on the structure and diffusion dynamics in the superionic state.[20] Nevertheless, it is envisaged that the present simulations will be extended to a shell model MD study of stabilised zirconia.

Table 1 Interatomic potentials for ZrO_2

(i) short-range

Interaction	A/eV	ρ/Å	C/eV Å^6
$Zr^{4+}\cdots O^{2-}$	985.869	0.3760	0.000
$O^{2-}\cdots O^{2-}$	22764.300	0.1490	27.890

(ii) shell model[a]

Species	Y/e	k/eV Å^{-2}
Zr^{4+}	1.350	169.617
O^{2-}	−2.077	27.290

[a] Y and k refer to the shell charge and harmonic force constant respectively. Note: region I = 300 ions; potential cut-off = 10.254 Å.

Table 2 Calculated and observed properties of cubic ZrO_2

(i) interatomic separations (Å)

Separation	r (calc.)	r (expt.)[a]	$\|\Delta\|$
Zr—O	2.176	2.204[a]	0.028
O—O	2.538	2.563[a]	0.025
Zr—Zr	3.620	3.589[b]	0.031

(ii) calculated properties of the perfect crystal

Property	ZrO_2
Lattice energy per formula unit/eV	−109.76
$a(=b=c)$/Å	5.076 (5.07)[c]
Elastic constants/10^{11} dyn cm^{-2}	
c_{11}	61.63 (40.09)[a]
c_{12}	11.96
c_{13}	11.96
c_{33}	61.63
c_{44}	10.08
c_{66}	10.08
Dielectric constants	
$\langle\varepsilon_0\rangle$	26.90 (29.3)[a]
$\langle\varepsilon_\infty\rangle$	2.63

[a] Ref. 15. [b] Ref. 29. [c] Ref. 3.

The MD simulations reported here were performed using the DLPOLY code with a simulation box comprising 2592 ions (*i.e.* $6\times6\times6$ fluorite unit cells) to which periodic boundary conditions were applied; the ensemble used imposes the conditions of constant temperature and pressure (NPT). The calculations were run using a time step (δt) of 10^{-15} s and for a total period of 50 ps including initial equilibration (of 3 ps). It is worth remarking that we are employing a longer time scale than the majority of previous MD simulations of polar solids. The doped system $Zr_{0.9}Y_{0.1}O_{2-\delta}$ was modelled by the partial substitution of Zr by Y (introduced at random) and the corresponding removal of oxygen ions as charge compensating vacancy defects.

Results and discussion

Dopant substitution

It is well established that the addition of aliovalent dopant ions (*e.g.* Ca^{2+}, Y^{3+}) to ZrO_2 acts to stabilise the high temperature cubic polymorph at ambient temperatures.[13] To maintain charge neutrality, anion vacancies are created which are distributed randomly in the lattice, and are the main reason for the outstanding ionic conduction exhibited by stabilised ZrO_2.[21–23] The most straightforward mode of dopant incorporation into the host lattice is as a substitutional ion at a Zr^{4+} site with compensating oxygen vacancies. This process of dopant substitution can be represented by the following defect equations:

$$MO + Zr_{Zr}^{X} + O_O^{X} \rightarrow M_{Zr}'' + V_O^{\bullet\bullet} + ZrO_2 \quad (2)$$

$$M_2O_3 + 2Zr_{Zr}^{X} + O_O^{X} \rightarrow 2M_{Zr}' + V_O^{\bullet\bullet} + 2ZrO_2 \quad (3)$$

where M_{Zr}'' and M_{Zr}' represent di- and tri-valent dopant substitution, respectively. From our simulation approach we can calculate systematically the energetics of these 'solution' reactions (E_{soln}) by combining the appropriate defect and lattice energy terms (U_L), which may yield predictive trends.

It is well documented that some of the most favourable dopants in ZrO_2 are the alkaline-earth and rare-earth ions.[1,3,4,5,7,24] Therefore, we have examined the substitution of these dopants into ZrO_2 in detail, as well as extending the study to include a range of other di- and tri-valent cations. Apart for the Cu^{2+}–O interaction,[25] the potential parameters for this set of dopants were taken from Lewis and Catlow,[26] and have been used in similar studies of other oxides.[14,25]

Our calculated energies of solution for the alkaline-earth dopants are plotted as a function of ion radius in Fig. 1. From an examination of the results it is apparent that the most favourable solution energy, and hence the highest solubility, is predicted for Ca^{2+}. Fig. 1 shows a strong degree of correlation between the solution energy and dopant size, with a minimum at Ca^{2+}. Moreover, our results are consistent with experimental studies that have demonstrated how the addition of Ca^{2+} to ZrO_2 not only stabilises the cubic phase, but improves ionic conduction.[4,5,7,15,22,24,27–36] It is noted that Mg^{2+} also shows a relatively low solution energy in ZrO_2 which suggests that this dopant could also be used as a stabiliser. However, experimental work has shown the instability of ZrO_2–MgO solid solutions at high temperatures.[5] The incorporation of Ba^{2+} (ionic radius 1.36 Å) into the host lattice is highly unfavourable, and this is probably due to the large 'mismatch' in ion size with the host Zr^{4+} (0.72 Å).

Similarly, the calculated solution energies for the rare-earth dopants (Y^{3+}, La^{3+}, Nd^{3+} and Gd^{3+}) are plotted *versus* dopant radius in Fig. 2. The lowest (and only negative) solution energy is calculated for Y^{3+}. Again Fig. 2 shows a clear minimum at this dopant, as well as a degree of correlation between the solution energy and dopant size. This result

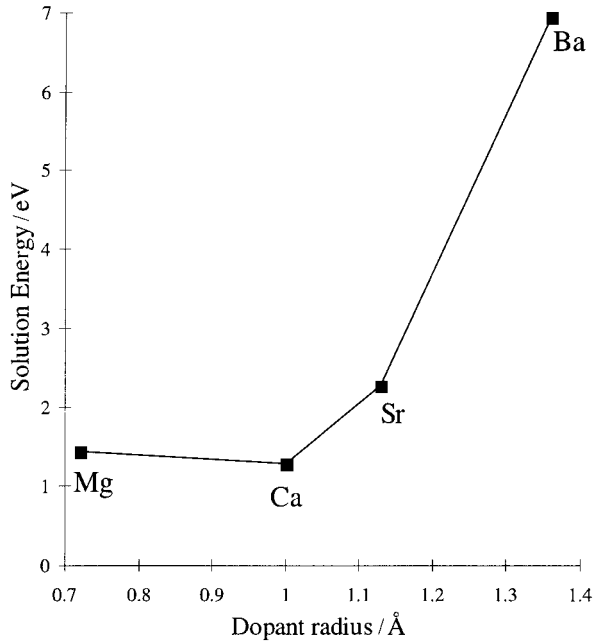

Fig. 1 Energies of solution for the alkaline-earth dopants as a function of dopant radius (the line is a guide to the eye).

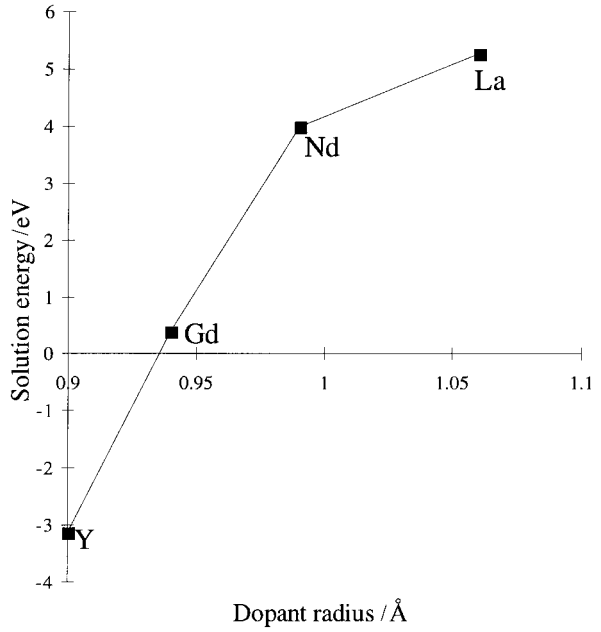

Fig. 2 Energies of solution for the rare-earth dopants as a function of dopant radius.

accords well with experimental work in which yttria-stabilised ZrO_2 is one of the most widely used solid electrolytes for applications requiring high oxygen ion conductivity.[5,7,12,13,24,37–43] Gd^{3+} also has a fairly favourable solution energy, and an ionic radius similar to Y^{3+}. However, to our knowledge there are no reports of ZrO_2–Gd_2O_3 being utilised for electrolyte applications, although Gd^{3+} is widely used as a dopant in the CeO_2-based oxygen ion conductor.[44,45]

A variety of cations are known to act as stabilisers in ZrO_2, preventing unfavourable transformations at lower temperatures.[46] As a possible predictive tool, we have incorporated a range of other cations (transition metal ions and Al^{3+}) into ZrO_2, and calculated the energetics of solution for these dopants. To our knowledge, this is the largest range of dopants in ZrO_2 that have been investigated using simulation techniques. Our calculated energies of solution for the di- and trivalent metals are plotted as a function of dopant size in Fig. 3.

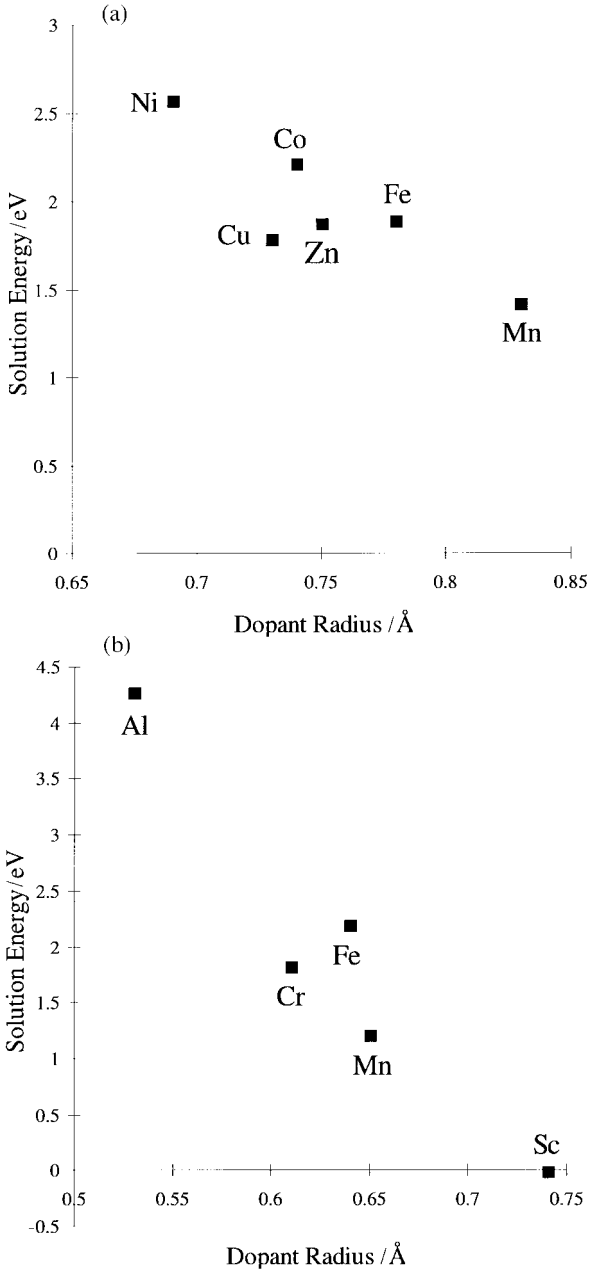

Fig. 3 Energies of solution as a function of dopant radius: (a) divalent ions, (b) trivalent ions.

From an examination of the results, Sc^{3+} exhibits the lowest solution energy which suggests that scandia-stabilised zirconia may be a promising electrolyte. Indeed, it has been shown that this material exhibits a higher conductivity than both yttria and calcia-stabilised zirconia.[5] However, Sc doped ZrO_2 is not widely utilised within SOFC configurations, largely due to cost considerations, although it may receive renewed interest if this factor is minimised. Experimental studies of Al_2O_3, Fe_2O_3 and Cr_2O_3 have found that the solubility of these compounds in ZrO_2 is relatively low and in the range of 0.6–3.0 mol%.[21,47]

Dopant-vacancy clusters

Previous conductivity and structural studies have established that interactions between dopant ions and their charge-compensating vacancies can lead to distinct dopant-vacancy clus-

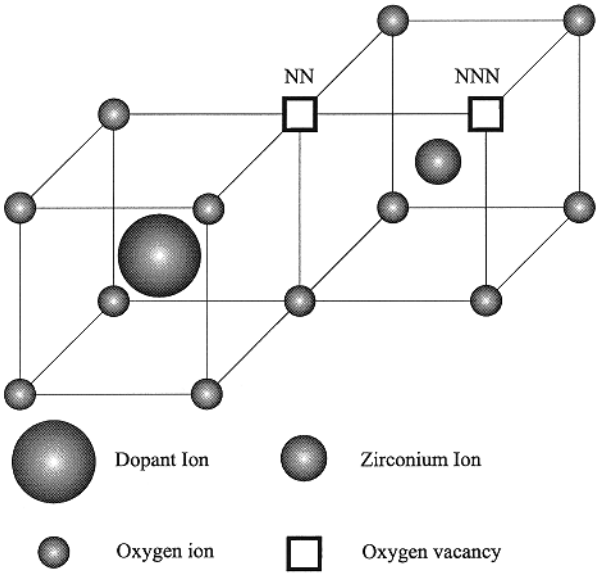

Fig. 4 Schematic diagram of simple pair clusters in ZrO_2 showing NN and NNN configurations.

ters. For example, in yttria doped ceria it has been shown that the conductivity is controlled by the extent of dopant-vacancy interactions.[18,44,45,48,49] This effect is believed to be due to the variation in the strength of the 'trapping' of the mobile oxygen vacancy by the dopant ion, which in turn has a strong effect on oxygen vacancy migration.[14] At low defect concentrations simple clusters are formed, which add a binding energy term to the Arrhenius energy of ionic conduction. It has been demonstrated, both experimentally and theoretically, that the elastic strain energy between the dopant and the oxygen vacancy is at least as important as the electrostatic term.[18,48,50]

Consequently, we have considered various cluster configurations in ZrO_2 involving the dopants considered above. The first set of clusters involve an oxygen vacancy located at either a nearest-neighbour (NN) or a next-nearest-neighbour (NNN) site to the dopant ion. These simple pair clusters are illustrated in Fig. 4. The cluster binding energies (with respect to isolated defects) are reported in Table 3 and have been calculated using the general relation:

$$E_{\text{bind}} = E_{\text{cluster}} - \left\{ \sum_{\text{component}} E_{\text{isolated defect}} \right\} \qquad (4)$$

Focusing on the results for the NN and NNN clusters, several interesting points arise. The negative binding energies indicate that the clusters are generally bound. In particular, the binding energy of -0.26 eV for Y^{3+} agrees well with a value of -0.28 eV derived from recent conductivity studies.[51] In addition, the stronger binding energy for Mn^{2+} in comparison with Mn^{3+} will enhance the solubility of Mn^{2+} to a greater extent, which is consistent with the observation of the Mn^{2+} state in ZrO_2.

In general, our results show that the larger ('oversized') dopants are more strongly bound to an oxygen vacancy at the NNN site, whereas the smaller trivalent metal ions generally favour the cluster with a NN vacancy. This observation can be explained in coordination terms: the trivalent metal dopants have a smaller radius than Zr^{4+} (0.72 Å) and prefer to be seven-fold coordinated. On the other hand, the larger dopants prefer to be eight-fold coordinated and therefore impose a cubic symmetry on the surrounding anion sub-lattice. This may be one of the reasons why the larger dopants act as good stabilisers of the cubic phase. Moreover, these observations are in agreement with recent X-ray absorption studies and theoretical work.[15,21] As a summary of our results, Fig. 5 illustrates the variation of the dopant-vacancy binding energies

Table 3 Binding energies for dopant-vacancy pair clusters

	E_{bind}/eV	
Dopant ion	NN	NNN
Alkaline-earths		
Mg^{2+}	−0.43	−0.45
Ca^{2+}	−0.31	−0.57
Sr^{2+}	−0.43	−0.69
Ba^{2+}	−0.79	−0.96
Rare-earths		
Y^{3+}	0.18	−0.26
La^{3+}	0.20	−0.40
Nd^{3+}	0.21	−0.36
Gd^{3+}	0.20	−0.30
Divalent metal dopants		
Mn^{2+}	−0.39	−0.49
Fe^{2+}	−0.42	−0.47
Co^{2+}	−0.44	−0.48
Ni^{2+}	−0.47	−0.49
Cu^{2+}	−0.58	−0.55
Zn^{2+}	−0.47	−0.51
Trivalent metal dopants		
Al^{3+}	−0.53	−0.37
Sc^{3+}	−0.04	−0.15
Cr^{3+}	−0.29	−0.28
Mn^{3+}	−0.26	−0.16
Fe^{3+}	−0.28	−0.19

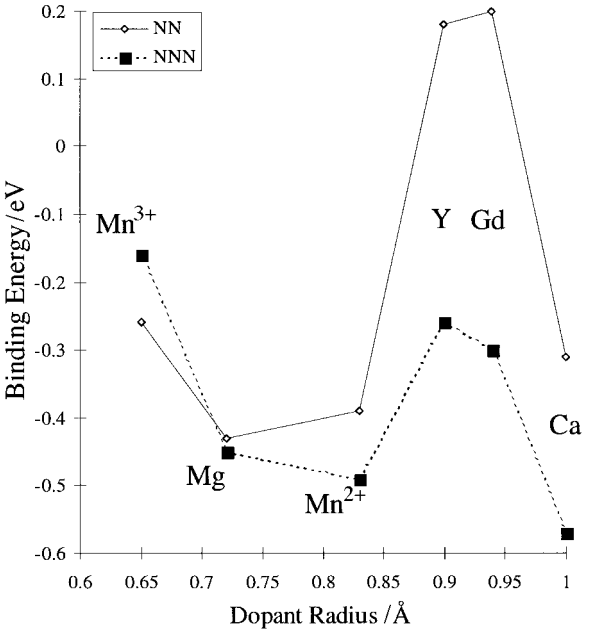

Fig. 5 Variation of dopant-vacancy binding energies with dopant radius for favourable dopants with the oxygen vacancy at both NN and NNN sites to the dopant ion.

with ion radius for the most favourable dopants (in terms of their solution energy). It is interesting to note that the 'cross-over' point in the stability of the NN and NNN configurations is at a radius of approximately 0.7 Å which corresponds closely to the radius of Zr^{4+} (0.72 Å). This is consistent with the view that Zr^{4+} is the smallest ion possible in maintaining the fluorite structure.[15,21]

Insertion of a dopant ion that differs in size to Zr^{4+} perturbs the surrounding host lattice,[12] which in turn may affect the mobility of a migrating oxygen. In previous sections we have shown that Ca^{2+}, Sc^{3+}, Mn^{2+} and Y^{3+} have the most favourable dopant solution energies. We have therefore examined, in detail, the local atomic structure around simple pair clusters involving these four dopants. As already noted, the

Table 4 Calculated and experimental interatomic separations for doped ZrO_2[a]

(a) oxygen vacancy located at an NN site to the dopant

Separation	r (calc.)/Å	r (expt.)/Å	$\|\Delta\|$
Ca—O	2.377	2.230[b]	0.147
Zr—O	2.117	2.120[b]	0.003
Zr—Ca	3.680		
Y—O	2.267	2.330[c]	0.340
Zr—O	2.119	2.150[c]	0.031
Zr—Y	3.724	3.580[c]	0.144
Mn—O	2.310		
Zr—O	2.047		
Zr—Mn	3.751		
Sc—O	2.185		
Zr—O	2.047		
Zr—Sc	3.746		

(b) oxygen vacancy located at an NNN site to the dopant

Separation	r (calc.)/Å	r (expt.)/Å	$\|\Delta\|$
Ca—O	2.437	2.230[b]	0.207
Zr—O	2.120	2.120[b]	0.000
Zr—Ca	3.550		
Y—O	2.340	2.330[c]	0.010
Zr—O	2.117	2.150[c]	0.033
Zr—Y	3.576	3.580[c]	0.004
Mn—O	2.394		
Zr—O	2.121		
Zr—Mn	3.597		
Sc—O	2.278		
Zr—O	2.119		
Zr—Sc	3.590		

[a]All separations refer to NN oxygen ions. [b]Ref. 21. [c]Ref. 12.

pair clusters are of the form $[M_{Zr}''\cdot V_O^{\bullet\bullet}]^X$ and $[M_{Zr}'\cdot V_O^{\bullet\bullet}]^{\bullet}$ for di- and tri-valent dopants, respectively, but maintain different local oxygen coordination. We have focused on clusters where the oxygen vacancy is located at either a NN or NNN site to the dopant (Fig. 4), and calculated the interatomic separations (Table 4).

Several key results emerge from our analysis. The average Zr—O bond lengths presented in Table 4 are lower than the Zr—O bond lengths in the pure crystal which is in accord with EXAFS measurements.[12] The dopant–oxygen bond length in the NN case is smaller than the dopant–oxygen bond length for the NNN configuration. This result can be accounted for by considering the coordination number of the dopant cation and the Zr^{4+} at the NN site: when either ion is in a seven-fold coordination a lower average bond length is expected. Li *et al.*[21] suggest that when an oxygen vacancy is sited NNN to the dopant cation, the zirconium–dopant bond length decreases to between 3.58 and 3.60 Å. Our results are in accord with this observation which give the mean zirconium–dopant bond length as 3.58 Å.

From the calculated data, we have also investigated the displacement of ions surrounding the dopant and our findings are depicted graphically in Fig. 6. The results are supported by XAS data[21] that find that oxygen ions adjacent to an oxygen vacancy are displaced towards it. We also find an off-centre displacement of the dopant cation, which is also consistent with the findings of Li *et al.*[21] The average displacement of oxygen ions that immediately surround the oxygen vacancy is calculated to be of the order of 0.4 Å. It is clear from this value that there is significant oxygen ion displacement within the defect cluster, confirming that these lower-valent dopants lead to considerable perturbation of the local structure.

Nb/Y co-doping

The anode material for solid oxide fuel cells should exhibit good mixed conducting properties at low oxygen partial pressures.[7] The combination of good oxygen ion conductivity with high electronic conductivity affords a greatly increased effective surface area for the electrode reaction and, hence improves efficiency.[52] Fluorite-based oxides, such as doped CeO_2 and stabilised ZrO_2, offer exceptionally high oxygen ion conductivity, and it is possible to induce electronic conductivity in reducing environments by doping these materials with early transition metals, *e.g.* Nb^{5+} and Ti^{4+}. However, the solubility of these ions is low in both CeO_2 and ZrO_2,[53,54] and large quantities are required to achieve a reasonable level of electronic conductivity. Such high levels of pentavalent dopant are also believed to be detrimental to ionic conductivity.

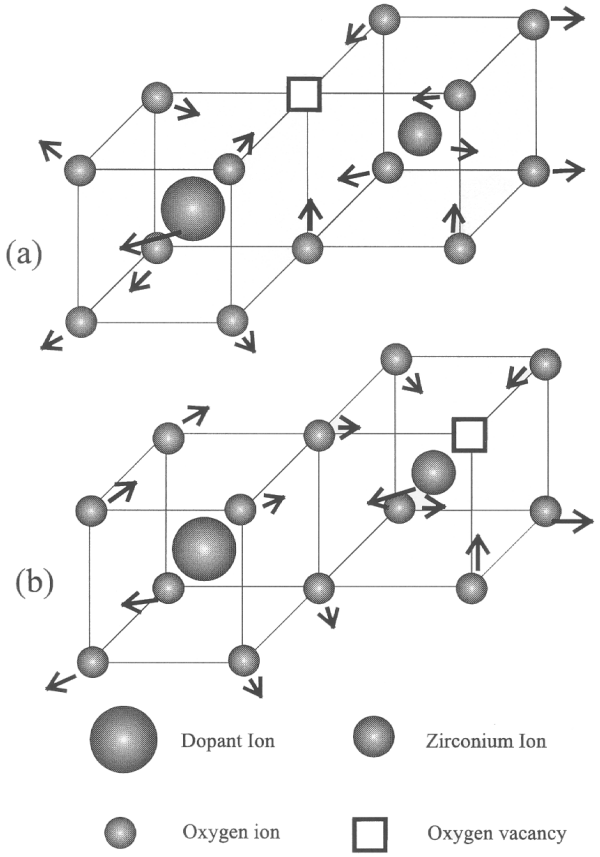

Fig. 6 Displacement of ions: (a) an oxygen vacancy at a NN site to the dopant, (b) an oxygen vacancy at a NNN site to the dopant.

A recent ac impedance spectroscopy and neutron powder diffraction study by Irvine *et al.*[51] proposed that co-doping with Nb^{5+} in cubic Y/ZrO_2 would be less detrimental to ionic conductivity based on electrostatic and size considerations. We have therefore carried out a preliminary study of the Nb_2O_5–Y_2O_3–ZrO_2 system. The GULP simulation code[16] has been employed which allows fractional occupancies to be specified for crystallographic sites, implemented through a mean field approach. This consists of scaling the interatomic potentials by the product of the site occupancies. For example, in the case of ZrO_2 containing Y^{3+}, this feature allows homogenous distributions of the dopant.

In the co-doped system two types of substitution can occur: zirconium being replaced by both the pentavalent niobium and the trivalent yttrium. Therefore, there will be three types of defect in this system: $Nb_{Zr}^{\bullet}$, Y_{Zr}' and $V_O^{\bullet\bullet}$. As a significant population of oxygen vacancies is required to stabilise the cubic fluorite structure, the concentration of trivalent dopant must always be significantly higher than that of the pentavalent ion.[51] For example, the defect equation for the incorporation

Table 5 Energies for isolated defects in $Zr_{1-x}Y_xO_{2-\delta}$

	Defect energy/eV	
x	$Nb_{Zr}^{\bullet}$	$V_O^{\bullet\bullet}$
0.00	−44.98	15.00
0.10	−43.37	15.64
0.25	−43.02	15.95

of the two dopants can be written as:

$$1/2Nb_2O_5 + 3/2Y_2O_3 + 4Zr_{Zr} + O_O^X \rightarrow Nb_{Zr}^{\bullet} + 3Y_{Zr}' + V_O^{\bullet\bullet} + 4ZrO_2 \quad (5)$$

where we have considered a higher level for Y doping. The use of the mean field approach involved an additional step in evaluating defect energies, which needs to be described briefly. If we assign M as the 'hybrid' Zr/Y cation present at each cation site of the $Zr_{1-x}Y_xO_{2-\delta}$ solid solution, then the substitution of a lattice Zr^{4+} with a Nb^{5+} must be preceded by the substitution of a 'hybrid' cation with a Zr^{4+} ion according to: $M_M^X \rightarrow Zr_M^X \rightarrow Nb_{Zr}^{\bullet}$. Using this approach allows us to set up a 'baseline' for our defect calculations. The resulting vacancy and substitution energies for various Y levels (x) in $Zr_{1-x}Y_xO_{2-\delta}$ are listed in Table 5. As with our previous dopant calculations, the energetics of solution for reaction (5) were evaluated from the following equation:

$$E_{soln} = E(Nb_{Zr}^{\bullet}) + 3(Y_{Zr}') + E(V_O^{\bullet\bullet}) + 4U_L(ZrO_2) - 1/2U_L(Nb_2O_5) - 3/2(Y_2O_3) \quad (6)$$

The resulting energies of solution are presented in Table 6; it is clear that as the yttria content increases from $x = 0.0$–0.25, there is a significant decrease in solution energy. The calculations therefore suggest that (on energetic grounds) the presence of yttrium promotes the solution of Nb^{5+} in zirconia. This is consistent with observation[51] which finds that the solubility of such pentavalent ions is low in pure ZrO_2, but is much higher when co-doped with di- or tri-valent cations. Extending the conductivity work on the $Nb/Y/ZrO_2$ system,[51] we have also investigated the local atomic structure around the Nb substitutional with the average displacements of lattice species reported in Table 7. The largest displacements occur for the nearest-neighbour (NN) oxygen ions, which can be rationalised in terms of ion size effects. The Nb^{5+} (0.64 Å) has a smaller ionic radius than the host cations and, as we have shown previously, this size mismatch can cause severe distortions of the surrounding anion sub-lattice. However, the perturbation of the local environment does not seem to be as severe as that calculated for the lower valent dopants such as Ca^{2+} and Mn^{2+}.

Table 6 Solution energy of Nb^{5+} in $Zr_{1-x}Y_xO_{2-\delta}$

x	E_{soln}/eV
0.00	3.24
0.10	−3.66
0.25	−3.00

Table 7 Average displacements due to the Nb dopant in $Zr_{0.9}Y_{0.1}O_{2-\delta}$

Species	Displacement/Å
Nb^{5+}	0.09
Y^{3+} and Zr^{4+} (NN)	0.09
O^{2-} (NN)	0.12
O^{2-} (NNN)	0.09

Oxygen diffusion in Y/ZrO_2

The solid electrolyte applications of yttria-stabilised zirconia (YSZ) stimulate interest in improving the fundamental understanding of the structure and dynamics of the mobile sublattice. Experimental conductivity measurements on YSZ utilising a variety of techniques that include low field dc conduction,[40] quasielectric light scattering,[37] impedance spectroscopy[55] and tracer diffusion methods[56] have found a maximum in the conductivity at about 8–10 mol% yttria doping.[57,58] In the simulation cell for our MD simulations, we therefore considered a Y^{3+} dopant level of 10% which was designated 10YSZ. On introducing the dopant ions, a charge imbalance arises which is compensated by the introduction of oxygen vacancies into the system. The simulations were carried out for a total of 50 ps (including 3 ps for equilibration) at a range of temperatures from 873–2073 K covering those that typically occur for fuel cell applications. We note that previous MD simulations of YSZ[59–61] have utilised smaller cells and shorter simulation times than the model used in the present study.

Structural information is obtained from the pair radial distribution function (RDF), which provides an insight into the long-range (dis)order of the crystal lattice. The cation–cation RDFs are shown in Fig. 7, which reveal a series of sharp, well ordered peaks corresponding to successive nearest-neighbour distances and typical of a crystalline solid. In contrast, the oxygen–oxygen RDF (Fig. 8) show weak, diffuse structure for separations greater than nearest-neighbour, indicating some loss of long-range order on the mobile oxygen sub-lattice. As the temperature increases from 1273–2073 K the first peak decreases in height, while subsequent peaks broaden suggesting greater disorder and increased oxygen diffusion at higher temperatures.

Within a solid oxide fuel cell configuration the thermal expansion of the electrolyte must be similar to the electrodes and interconnect materials, otherwise the cell may fracture.[7] For example, the typical anode material is a Ni/YSZ cermet which has a thermal expansion coefficient of about $12 \times 10^{-6}\ K^{-1}$,[62] which is close to that of YSZ. Our results reveal that the process of thermal expansion over the simulation temperature range is fairly linear. From these we derive a thermal expansion coefficient of $11.09 \times 10^{-6}\ K^{-1}$, which compares well with an observed value[7] for YSZ of $10.5 \times 10^{-6}\ K^{-1}$.

Atomic transport properties are extracted from the simulations using the time-dependent mean square displacement (MSD), which are defined in the usual way,

$$\langle r_i^2(t) \rangle = \frac{1}{N} \sum_{i=1}^{N} [r_i(t) - r_i(0)]^2 \quad (7)$$

where N is the total number of ions in the system. In the perfect lattice, the MSD of component ions usually oscillates about a mean value. However, in a defective lattice, where there is a mobile species, such as O^{2-} in stabilised zirconia, the MSD increases with time. In Fig. 9, the MSD data are plotted as a function of time for 10YSZ at 1273 K. After the initial equilibration, the cation functions rapidly tend to a constant value with time, which confirms that cation diffusion is insignificant in 10YSZ. In contrast, the oxygen function increases rapidly as a function of time, indicating appreciable ion diffusion. Therefore, it is clear that the presence of yttria as a stabiliser in zirconia enhances oxygen ion diffusion. Fig. 10 depicts the MSD of oxygen ions at 1273, 1773 and 2073 K in which the cations have been omitted for clarity. It is apparent that with an increase in temperature there is an accompanied increase in oxygen diffusion.

From the slope of the MSD plot we may obtain the diffusion coefficient (D_i) according to the well known relationship:

$$\langle r_i^2(t) \rangle = 6D_i t + B_i \quad (8)$$

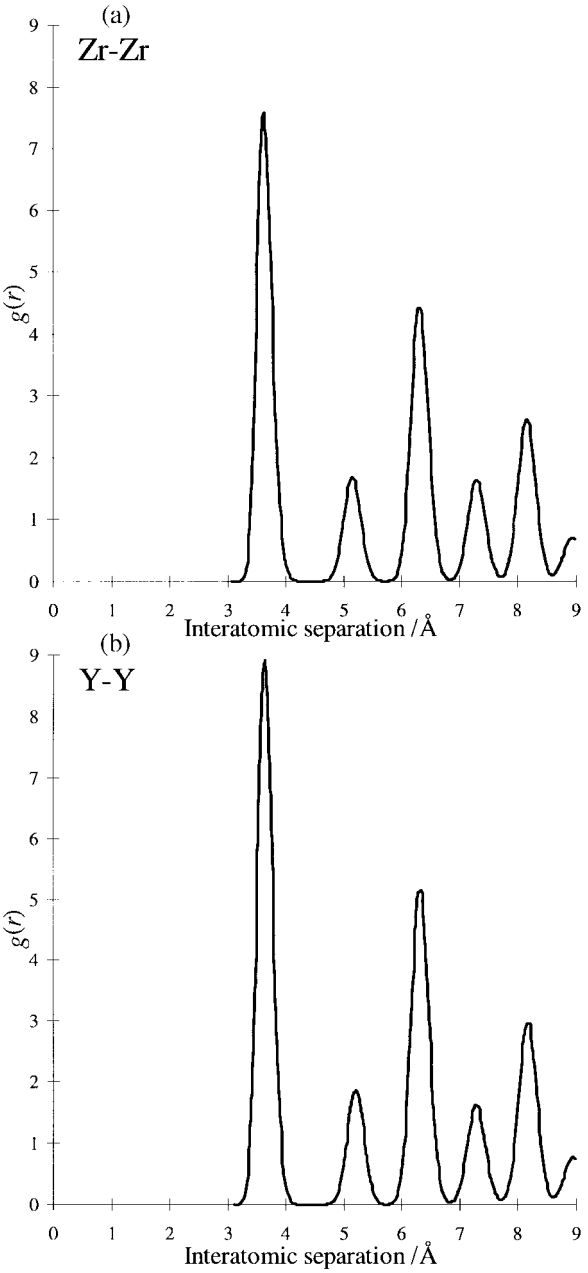

Fig. 7 Radial distribution functions in 10YSZ at 1273 K: (a) Zr–Zr, (b) Y–Y.

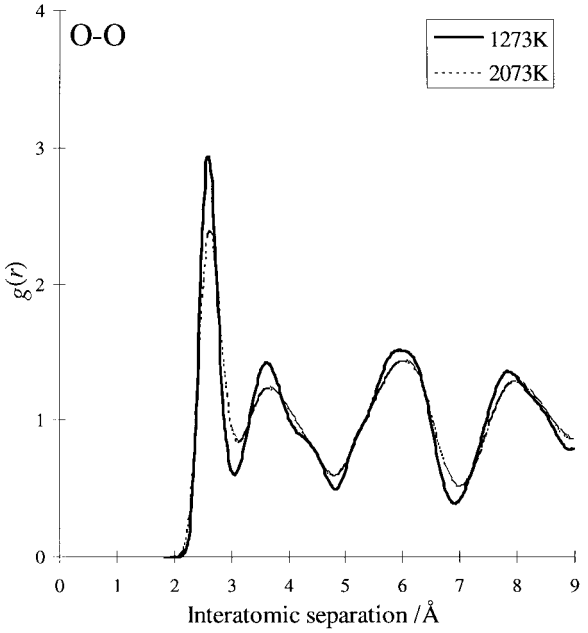

Fig. 8 Radial distribution function for O—O in 10YSZ at 1273 and 2073 K.

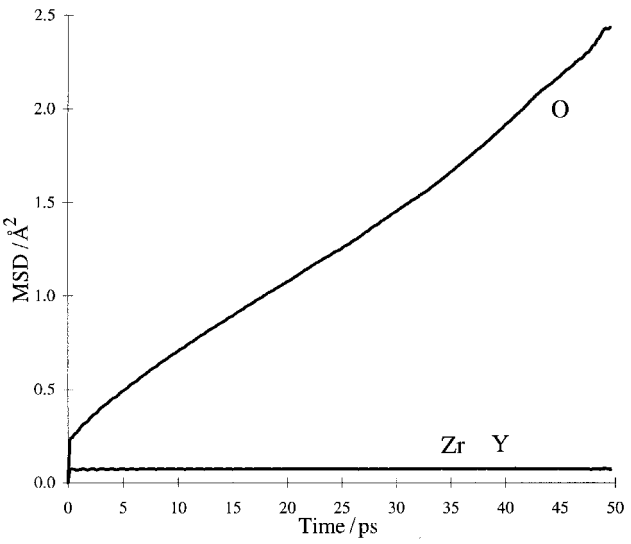

Fig. 9 Mean square displacement of all ion species in 10YSZ at 1273 K.

where B is the small thermal factor arising from atomic vibrations. The calculated diffusion coefficients at all simulation temperatures are listed in Table 8. From the calculated diffusion data we may evaluate an activation energy for oxygen migration using the standard Arrhenius relation:

$$D = A \exp(-E_{act}/kT) \quad (9)$$

where E_{act} is the activation energy. Fig. 11 shows a Arrhenius plot (ln D *vs.* $1/T$), onto which data from experimental and previous theoretical studies have been included. Our calculated slope is compatible with the available tracer experiments of Oishi and Ando[56] and the simulations of Li and Hafskjold.[59] Moreover, we find good quantitative agreement with calculated values at the highest temperature of 2073 K from studies of Okazaki *et al.*[61] and Shimojo *et al.*[60] We should note that our simulations have covered a wider temperature range than the tracer diffusion experiments[56] and previous simulation studies.[58,59]

From our data in Fig. 11 we derive an activation energy of 0.37 eV. This value is in reasonable agreement with an activation energy of 0.44 eV derived from tracer diffusion experiments.[56] Our results are also consistent with the MD study by Li and Hafskjold[59] which employed several sets of potential parameters and found that the calculated diffusion coefficients yielded activation energies in the range of 0.2–0.8 eV. However, our value is generally lower than activation energies derived from bulk conductivity and ac impedance spectroscopy measurements which show significant scatter: values range from 0.79–1.12 eV.[9,22,63] One reason for this variation could be the incorporation of a binding energy term which arises from the 'trapping' of oxygen vacancies by the Y^{3+} dopant to form defect clusters as discussed above. It is also worth noting that a study by Adler and Smith[64] on oxygen transport in fluorite-structured Y/CeO_2 found an activation energy of 0.49 eV, with a corresponding binding energy of 0.49 eV.

It is envisaged that the investigation presented here will be extended to encompass surface exchange processes, surface segregation of dopants and oxygen ion diffusion (using shell model MD).

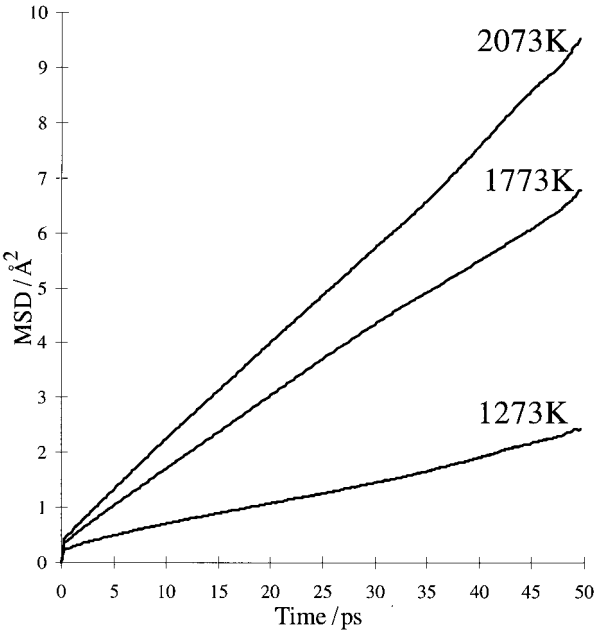

Fig. 10 Mean square displacement of oxygen ions in 10YSZ at 1273, 1773 and 2073 K.

Table 8 Calculated oxygen diffusion coefficients in 10YSZ

Temperature/K	$D_o/10^{-6}$ cm^2 s^{-1}
873	0.19
1073	0.34
1273	0.70
1773	2.12
2073	3.00

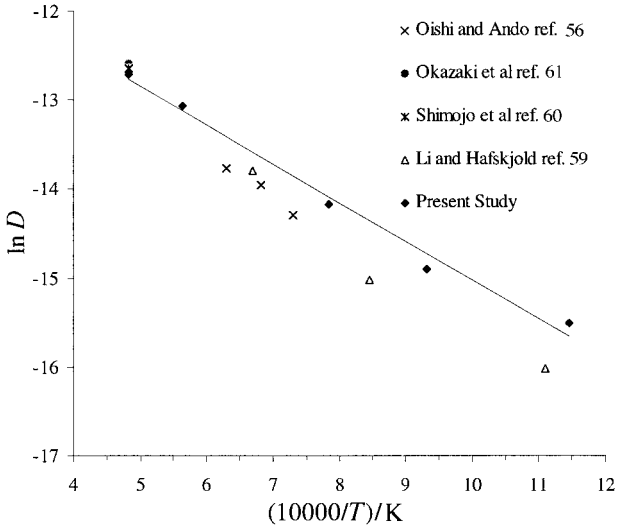

Fig. 11 Arrhenius plot for 10YSZ.

Conclusion

The present study of ZrO_2 has used both defect simulation and MD techniques, and forms part of the continuing effort to improve our understanding of the bulk defect and oxygen ion transport properties at the atomic level. The following points have emerged from our results:

(1) Favourable dopants (on energetic grounds) are calculated to be: CaO, MnO, Y_2O_3, Gd_2O_3 and Sc_2O_3. The 'solution' of these dopants will enhance oxygen diffusivity owing to the increase in the oxygen vacancy concentration. These results agree well with conductivity and diffusion experiments in which these dopants are used to enhance oxygen ion conductivity in zirconia.

(2) The calculations on defect clusters find that cation dopants with a larger ionic radii than the host Zr^{4+} prefer the charge-compensating oxygen vacancy to be at a next-nearest-neighbour (NNN) site, leaving them in an eight-fold coordination; conversely 'undersized' dopants prefer the vacancy to be situated at nearest-neighbour (NN) positions. Moreover, these results together with the calculated ion displacements are consistent with EXAFS studies of the local atomic structure.

(3) From our calculations on Nb/Y co-doping we have shown how the presence of yttria greatly promotes the solution of Nb^{5+} into cubic zirconia. We have also shown that Nb substitution for zirconium leads to small distortions in the surrounding anion sub-lattice.

(4) The pair distribution functions from the MD simulations show considerable disorder in the oxygen sub-lattice. The degree of disorder increases with increasing temperature associated with enhanced oxygen diffusion.

(5) Oxygen diffusion coefficients have been calculated for Y/ZrO_2 and rise to the order of 3×10^{-6} cm^2 s^{-1} at 2073 K indicating rapid oxygen transport. Ion diffusion was not observed within the undoped system, confirming the need for yttria stabilisation for appreciable oxygen ion conductivity. Our MD study has covered a wider range of temperatures than previous experimental and simulation work on this system.

We thank W. Smith and A. Dicks for valuable discussions. This work was financially supported by BG plc (Gas Research and Technology Centre). The simulations were performed on the computing facilities at ULCC and at the Daresbury Laboratory.

References

1 B. C. H Steele, *Mater. Sci. Eng. B*, 1992, **13**, 79; B. C. H. Steele, *Solid State Ionics*, 1995, **75**, 157.
2 W. J Weber, H. L. Tuller, T. O. Mason and A. N. Cormack, *Mater. Sci. Eng. B*, 1993, **18**, 52.
3 C. R. A. Catlow, *J. Chem. Soc., Faraday Trans.*, 1990, **86**, 1167.
4 E. C. Subbarao and H. S. Maiti, *Solid State Ionics*, 1984, **11**, 317.
5 T. H. Etsell and S. N. Flengas, *Chem. Rev.*, 1970, **70**, 339.
6 A. J. Moulson and J. M. Herbert, *Electroceramics: Materials, Properties and Applications*, Chapman and Hall, London, 1990.
7 N. Q. Minh, *J. Am. Ceram. Soc.*, 1993, **76**, 563.
8 J. Kilner, S. Benson, J. Lane and D. Waller, *Chem. Ind. (London)*, 1997, **22**, 907.
9 I. R. Gibson and J. T. S. Irvine, *J. Mater. Chem.*, 1996, **6**, 895.
10 M. Moringa, J. B. Cohen and F. Faber, *Acta Crystallogr., Sect. A*, 1979, **35**, 789; 1980, **36**, 520.
11 D. Steele and B. E. F. Fender, *J. Phys. C*, 1974, **7**, 1.
12 C. R. A. Catlow, A. V. Chadwick, C. N. Greaves and L. M. Moroney, *J. Am. Ceram. Soc.*, 1986, **69**, 272.
13 B. W. Veal, A. G. McKale, A. P. Paulikas, S. J. Rothman and L. J. Nowicki, *Physica B*, 1988, **150**, 234.
14 M. S. Islam, M. Cherry and L. J. Winch, *J. Chem. Soc., Faraday Trans.*, 1996, **92**, 479.
15 A. Dwivedi and A. N. Cormack, *Philos. Mag. A*, 1990, **61**, 1.
16 J. D. Gale, *Philos. Mag. B*, 1996, **73**, 3; *J. Chem. Soc., Faraday Trans.*, 1997, **93**, 629.
17 W. Smith and T. R. Forester, *J. Mol. Graphics*, 1994, **14**, 136.
18 C. R. A. Catlow, *Solid State Chemistry: Techniques*, ed. A. K. Cheetham and P. Day, Clarenden Press, Oxford, 1987.
19 M. P. Allen and D. J. Tildesley, *Computer Simulation of Liquids*, Oxford University Press, Oxford, 1987.
20 P. J. D. Lindan and M. J. Gillan, *J. Phys.: Condens. Matter*, 1993, **5**, 1019.
21 P. Li, I. Chen and J. E. Penner-Hahn, *J. Am. Ceram. Soc.*, 1994, **77**, 118; *J. Am. Ceram. Soc.*, 1994, **77**, 1281; P. Li and I. Chen, *J. Am. Ceram. Soc.*, 1994, **77**, 1289.
22 A. Orliukas, P. Bohac, K. Sasaki and L. J. Gauckler, *Solid State Ionics*, 1994, **72**, 35.
23 A. Weyl and D. Janke, *J. Am. Ceram. Soc.*, 1997, **80**, 861.

24 J. F. Baumard and P. Abelard *Adv. Ceram.*, 1984, **12**, 46.
25 R. C. Baetzold, *Phys. Rev. B*, 1988, **38**, 11304.
26 G. V. Lewis and C. R. A. Catlow, *J. Phys. C*, 1985, **18**, 1149.
27 B. Cales and J. F. Baumard, *J. Mater. Sci*., 1982, **17**, 3243.
28 B. Strauß, H. Boysen, F. Frey, U. Steigenberger, F. Güthoff, A. Krimmel, H. M. Mayer and D. Welz, *J. Phys.: Condens. Matter*, 1995, **7**, 7823.
29 M. Ruhle and H. Heuher, *Adv. Ceram*., 1984, **12**, 14.
30 J. Corish, *J. Chem. Soc.*, *Faraday Trans. 2*, 1989, **85**, 437.
31 C. R. A. Catlow, J. Corish, K. M. Diller, P. W. M. Jacobs and M. J. Norgett, *J. Phys. C: Solid State Physics*, 1979, **12**, 451.
32 W. C. Mackrodt and P. M. Woodrow, *J. Am. Ceram. Soc*., 1986, **69**, 277.
33 S. Dou, C. R. Mason and P. D. Pacey, *Solid State Ionics*, 1986, **18–19**, 736.
34 T. Y. Tien and E. C. Subbarao, *J. Chem. Phys*., 1963, **39**, 1041.
35 H. J. Rossel, J. R. Seller and I. J. Wilson, *Acta Crystallogr.*, *Sect. B*, 1991, **47**, 862.
36 T. He, K. D. Becker and D. S. Tannhauser, *Ber. Bunsenges. Phys. Chem*., 1995, **99**, 658.
37 T. Suemoto and M. Ishigame, *Solid State Ionics*, 1986, **21**, 225.
38 C. R. A. Catlow, A. V. Chadwick, A. N. Cormack, G. N. Greaves, M. Leslie and L. M. Moroney, *Mater. Res. Soc. Symp. Proc*., 1986, **60**, 173.
39 M. Aoki, Y. Chiang, I. Kosacki, L. J. Lee, H. L. Tuller and Y. Liu, *J. Am. Ceram. Soc*., 1996, **79**, 1169.
40 R. E. W. Casselton, *Phys. Status Solidi A*, 1970, **2**, 571.
41 D. Gomez-Garcia, J. Martinez-Fernandez, A. Dominguez-Rodriguez and J. Castang, *J. Am. Ceram. Soc*., 1997, **80**, 1068.
42 J. W. Adams, R. Ruh and K. S. Mazdiyasni, *J. Am. Ceram. Soc*., 1997, **80**, 903.
43 M. C. Steil, F. Thevenot and M. Kleitz, *J. Electrochem. Soc*., 1997, **144**, 390.
44 V. Butler, C. R. A. Catlow, B. E. F. Fender and J. H. Harding, *Solid State Ionics*, 1983, **8**, 109.
45 P. Li, I. Chen, J. E. Penner-Hahn and T. Tien, *J. Am. Ceram. Soc*., 1991, **74**, 958.
46 T. S. Sheu, T-Y. Tien and I-W. Chen., *J. Am. Ceram. Soc*., 1992, **75**, 1108.
47 X. Guo and R. Yuan, *J. Mater. Sci*., 1995, **30**, 923.
48 R. Gerhardt-Anderson and A. S. Nowick, *Solid State Ionics*, 1981, **8**, 89.
49 S. B. Adler and J. W. Smith, *J. Chem. Soc.*, *Faraday Trans*., 1993, **89**, 3123.
50 J. A. Kilner and R. J. Brook, *Solid State Ionics*, 1982, **6**, 237
51 J. T. S. Irvine, I. R. Gibson and D. P. Fagg, *Ionics*, 1995, **1**, 279.
52 H. Uchida, M. Yoshhida and M. Watanba, *J. Phys. Chem.*, 1995, **99**, 3282.
53 I. K. Naik and T. Y. Tien, *J. Electrochem. Soc*., 1979, **126**, 562.
54 R. S. Roth and L. W. Coughanour, in *Phase Diagrams for Ceramists: Volume 1*, ed. E. M. Levin, C. R. Robbins and H. F. McMurdie, American Ceramic Society, Columbus OH, 1964.
55 P. Abelard and J. F. Baumard, *Phys. Rev. B*., 1982, **26**, 1005.
56 Y. Oishi and K. Ando, *Transport in Nonstoichiometric Compounds*, ed. G. Simovich and V. S. Stubican, NATO ASI Ser. B 129, 1985.
57 S. P. S. Badwal, *J. Mater. Sci*., 1985, **20**, 4593.
58 S. P. S. Badwal, *Solid State Ionics*, 1992, **52**, 23.
59 X. Li and B. Hafskjold, *J. Phys*.: *Condens. Matter*, 1995, **7**, 1255.
60 F. Shimojo, H. Okazaki, T. Okabe, F. Tachibana and M. Kobayashi, *J. Phys. Soc. Jpn*., 1992, **61**, 2848; F. Shimojo and H. Okazaki, *J. Phys. Soc. Jpn.*, 1992, **61**, 4106.
61 H. Okazaki, H. Suzuki and K. Ihata, *Physics Lett. A*, 1994, **188**, 291; H. Okazaki, H. Suzuki and K. Ihata, *J. Phys. Soc. Jpn*., 1994, **63**, 3556.
62 S. Majumdar, T. Claar and B. Flandermayer, *J. Am. Ceram. Soc*., 1986, **69**, 628.
63 I. R. Gibson, E. E. Lachowski, J. T. S. Irvine and G. P. Dransfield, *Solid State Ionics*, 1994, **72**, 265.
64 S. B. Adler and J. W. Smith, *J. Chem. Soc.*, *Faraday Trans*., 1993, **89**, 3123.

Paper 8/03917H